J Mater Sci (2009) 44:1427–1434
DOI 10.1007/s10853-008-3168-y

SYNTACTIC AND COMPOSITE FOAMS

Morphology and properties of injection-moulded carbon-nanofibre poly(etheretherketone) foams

Raquel Verdejo · Philipp Werner · Jan Sandler · Volker Altstädt · M. S. P. Shaffer

Received: 29 February 2008 / Accepted: 5 December 2008 / Published online: 15 January 2009

Abstract Poly(ether ether ketone) (PEEK) is a high performance polymer that cannot usually be foamed reliably using conventional injection-moulding processes. Here, vapour-grown carbon nanofibres (CNFs) are introduced to stabilise the foaming process, and the resulting morphology of injection-moulded integral foams is investigated in detail. Different image analysis techniques revealed the positive effect of the nanofiller on the cellular structure. Electron microscopy confirmed a homogeneous dispersion of the nanofibres in the cellular PEEK cores. The mechanical properties of the foam injection-moulded samples, in bending, showed an increase in yield strength and elastic modulus with nanofibre loading fractions up to 15 wt%. Although the compressive properties of the foams were reduced as compared to the solid-polymer, the CNFs clearly offset this reduction in properties. Detailed differential scanning calorimetry (DSC) and dynamic mechanical analysis provide further evidence of an interaction between the matrix and the nanoscale filler.

R. Verdejo · M. S. P. Shaffer (✉)
Department of Chemistry, Imperial College London, London SW7 2AZ, UK
e-mail: m.shaffer@imperial.ac.uk

Present Address:
R. Verdejo
Institute of Polymer Science and Technology, CSIC, Juan de la Cierva 3, 28006 Madrid, Spain
e-mail: rverdejo@ictp.csic.es

P. Werner
Lehmann & Voss & Co. KG, Schimmelmannstr. 103, 22043 Hamburg, Germany

J. Sandler · V. Altstädt
University of Bayreuth, Universitätsstraße 30, 95440 Bayreuth, Germany

Introduction

The addition of carbon nanotubes (CNTs) and carbon nanofibres (CNFs) to polymer matrices has already been shown to improve their mechanical, electrical and thermal properties [1, 2]. However, progress has been partly limited by the availability of high-quality nanomaterials and partly by fundamental composite issues relating to dispersion, alignment, and interfacial adhesion. More recently, it has become apparent that immediate opportunities lie in introducing CNTs/CNFs into systems where conventional reinforcing fibres cannot be physically accommodated. Successful examples include polymer films [3–14], fibres [14–19] and matrices of conventional fibre composites; here, the focus is on polymer foams.

Polymeric foams are important and versatile materials due to their outstanding strength–weight ratio, their resilience, and their electrical, thermal and acoustic insulation properties, amongst other characteristics [20]. The foamability of a thermoplastic is related to the rheology of the melt, which mainly determines the stability of the growing cellular structure against collapse and/or the coalescence of the individual bubbles during the expansion process. Typically, semicrystalline thermoplastic polymers are difficult to foam because they usually have low shear and elongational viscosities, above the

melting temperature. At the same time, the melt rheology cannot be improved by simple cooling due to the onset of crystallisation.

Recently, nanoclays and various other nanoparticles [21–29] have been used as reinforcements for polymeric foams as they can be completely embedded in the polymer matrix without disrupting its cellular structure. It has been suggested that, in some cases, the nanofiller may act as a nucleation agent; however, there is also clear evidence that such nanoscale fillers can also significantly alter the relevant rheological properties of the melt. The properties of CNF- or CNT-reinforced polymeric foams have, as yet, received minimal attention, although initial studies have reported on CNT/polystyrene [30–34], CNF/PEEK [35] systems. These carbon nanostructures, with their excellent mechanical properties and high aspect ratios, have particular potential both to modify the foaming processes and to enhance the mechanical performance of the final cellular composite.

Previously [35], we reported that CNF-PEEK compounds have substantially increased melt strength without showing significantly reduced melt elongation properties. The CNFs were able to enhance the extensional flow behaviour of semicrystalline poly(ether ether ketone) (PEEK), at temperatures above the crystallisation point, thereby enabling the production of integral CNF-reinforced PEEK foams using an injection-moulding process. Previous studies show that solid PEEK-CNF samples have improved mechanical properties and wear performance [36, 37]. Furthermore, the reinforcing effect in melt spun PEEK-CNF fibres was more pronounced than for injection-moulded samples, suggesting that a high degree of shear alignment may be beneficial [18].

Foam injection moulding (FIM) is a cost efficient and effective means of producing components with an integral solid skin around a cellular foamed inner core. The resulting structure is lighter and less expensive than other, dense plastics; however, conventional reinforcements such as glass fibres are difficult to accommodate without damaging the cellular structure [38]. As such, nanofibres have great potential to simultaneously improve both processing methods and properties, through the formation of nanofibre-reinforced struts.

The aim of the present study was to investigate these effects in detail, in particular the influence of the nanofiller on the cellular structure, morphology and properties of CNF-reinforced PEEK foams. The melt rheology of this CNF/PEEK system has been reported elsewhere, along with a brief summary of the foaming process [35]. Here, we provide a detailed analysis of the properties of the foam products and the effects on the polymer microstructure, including a comparison of two different blowing agents, Clariant XH907 and $Al(OH)_3$.

Experimental

Foam preparation and characterisation

Poly(ether ether ketone) nanocomposite masterbatches containing 0, 5 and 10 wt% CNF were prepared using a Berstorff co-rotating twin-screw extruder with a length-to diameter ratio of 33 [36]. These masterbatches were dry mixed with 1 wt% of two different blowing agents, $Al(OH)_3$ and Clariant XH907. This mix was then fed into an Arburg Allrounder 420 injection-moulding machine for the moulding of flexural bars (according to ASTM D790 standard, 10 mm × 4 mm × 80 mm) at processing temperatures of 360 °C, with the mould temperature set to 100 °C [35]. Prior to analysis, the samples were heat-treated at 200 °C for 30 min followed by 4 h at 220 °C to ensure a similar degree of crystallinity [36].

The resulting integral foam samples were fractured in a plane perpendicular to the elongational flow direction and examined by optical microscopy. Afterwards, the cellular structure was examined by scanning electron microscopy (SEM) using a JEOL JSM 5610 after vacuum-coating with gold. Image analysis was performed on both optical and SEM images using ImageJ software, using Feret's diameter as a measure of the average cell size. Prior to the analysis, a manual tracing of the cell structure was performed and a greyscale image was obtained from scanning the outlined structure. The mean cell size was the average measured from three different regions with a minimum of 300 cells per foam for filled Clariant samples and 20 cells per foam for the the other samples, with larger cell sizes. In addition, a Skyscan X-ray microtomograph 1072 (μ-CT) with a maximum spot resolution of 5 μm (operating at a voltage of 79 kV and a current of 94 μA) was used to evaluate the morphology of the integral foams over a length of about 1 cm. The moulded specimens were examined using the cone-beam technology; 2-dimensional (2D) cross-sectional images were taken in steps of 0.23° up to a complete sample rotation of 360°. Although the set of 2D images can routinely be reconstructed to provide 3-dimensional (3D) volumetric images using the proprietary software "NRecon" from Skyscan, the individual 2D images were used here to visualise a representative plane through the complete cross-section of the moulded specimens.

Three-point bending tests were carried out according to ASTM D790 M at room temperature, using an Instron universal testing machine at a crosshead speed of 2 mm/min and a span of 64 mm (L/d = 16). The compressive strength of the foams was also analysed at a crosshead speed of 2 mm/min. The foam core of the original samples was exposed by mechanically removing 1 mm from the sides of the bars, i.e. the compression samples had a sandwich (solid–foam–solid) structure.

Dynamic mechanical thermal analysis (DMTA) was carried out on samples with an unambiguous cellular structure, using a Triton system between 25 and 300 °C at a heating rate of 5 °C/min; experiments were performed at a frequency of 1 Hz in 3-point bending mode. Three samples (average mass 7.0 ± 0.2 mg) were cut from both the skin and core of the flexural bars. Differential scanning calorimetry (DSC) analysis was carried out using Diamond 1 Perkin Elmer equipment; crystallisation and melting patterns were recorded at 10 °C/min between 75 and 380 °C.

Results and discussion

Inspection of the fractured foam samples (Fig. 1a) optically and by X-ray micro-tomography (Fig. 3) confirms that the pure PEEK does not foam reliably, under the chosen processing conditions, forming only a few large bubbles within the volume of the rectangular bar. The addition of CNFs to the PEEK, however, leads to the evolution of a homogeneous cellular morphology in the core of the integral structure that is associated with a simultaneous decrease in size and increase in number of cells. The degree of improvement of the foam morphology is strongly affected by the nature of the chemical blowing agent used; the Clariant foaming agent was much more successful than $Al(OH)_3$. As can be seen (Fig. 1), all of the CNF-Clariant samples had a homogeneous cellular structure in the core and a 1-mm solid surrounding skin. This promising integral structure is not present in the unfilled PEEK sample; the $Al(OH)_3$ samples (Fig. 1b) also have larger bubbles, but nevertheless show a decreasing bubble size with increasing CNF content (Fig. 2) [35]. The relative success of the

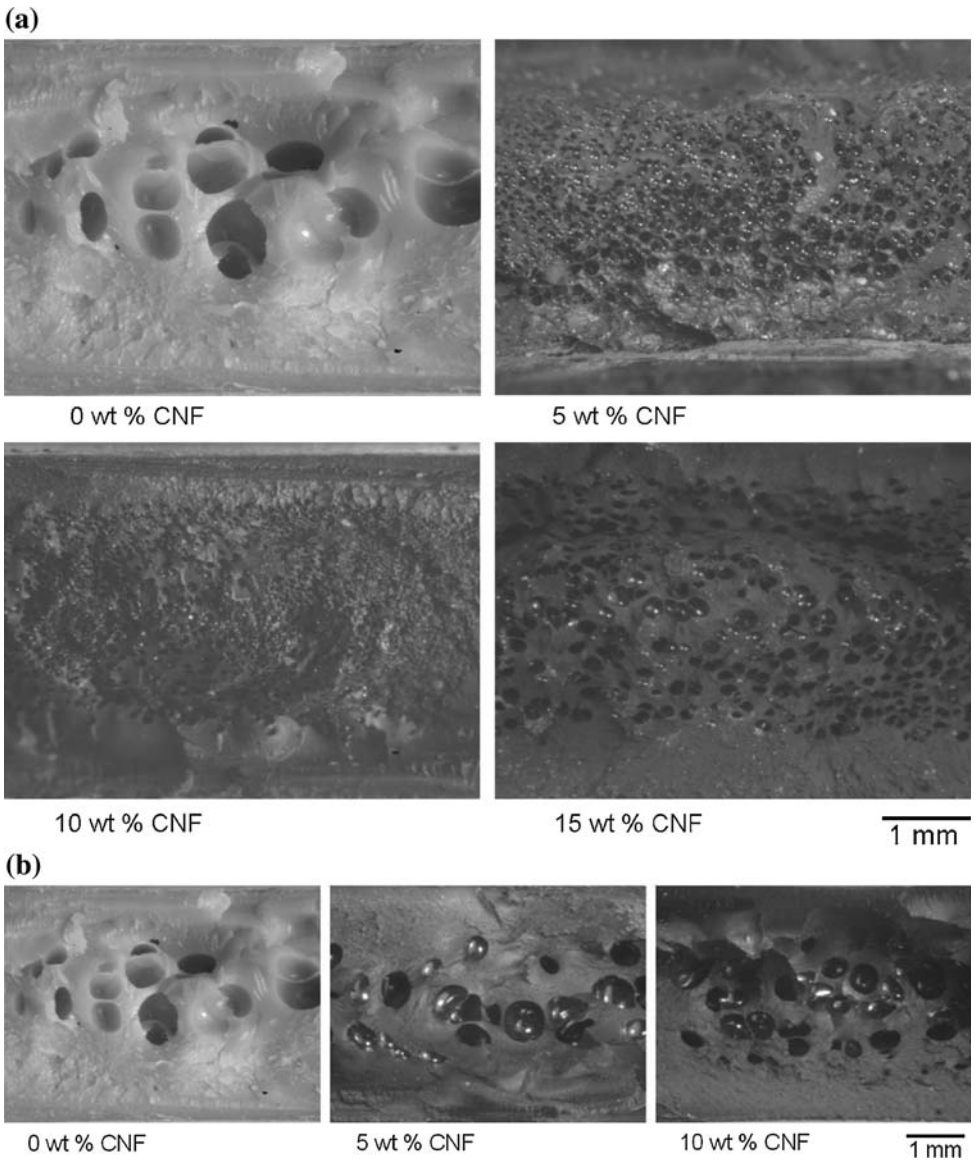

Fig. 1 Optical light microscopy images of the fracture surfaces of FIM samples produced using **a** Clariant XH907 and **b** $Al(OH)_3$ as blowing agents, at different CNF loading fractions

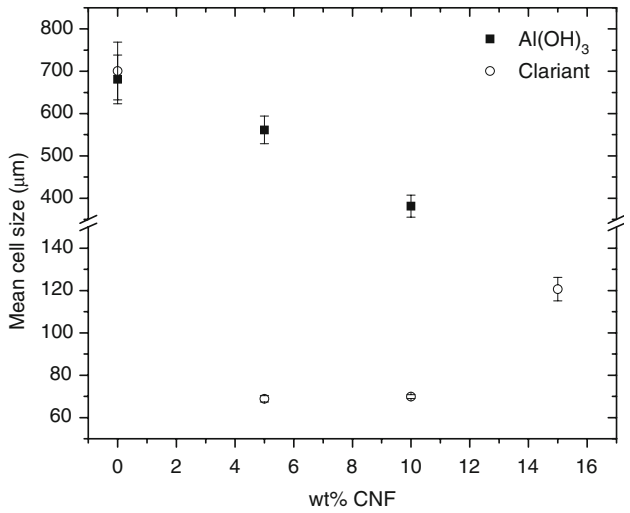

Fig. 2 Plot showing the mean cell size and standard deviation of cells in the foam cores of the integral PEEK-CNF samples

prototype Clariant system may simply reflect an improved distribution of the blowing agent which is relatively compatible with the polymer, but is more likely due to the production of CO_2 rather than H_2O as the blowing gas, which is more soluble in PEEK. The difference cannot be attributed to variations in the decomposition temperature, as $Al(OH)_3$ is known to decompose from around 230 °C, whilst Clariant compound decomposes from 216 °C (TGA data, not shown). Significantly higher processing temperatures are reached at early stages during the injection-moulding process, thereby providing sufficient time for dissolution of the released gas. Similar reductions in cell size have been observed in more easily foamed polymers filled with nanoclays, including polyamide [21, 22] and polystyrene and poly(methylmethcrylate) [27] foams. Nucleation effects may explain a reduction in cell size but do not explain the stabilisation of the PEEK foams, which must also relate to the increased melt strength.

Scanning electron microscopy analysis of the CNF-Clariant samples indicates a gradual change of the cellular structure along the cross-section normal to the melt flow direction (Fig. 3). Uniform rounded cells are concentrated around the centre of the sample, whilst cells closed to the solid skin are elongated where the shear flow is more pronounced. Similar effects have also been observed in polyamide-nanoclay foams [21, 22]. Image analysis was performed of the cells around the centre of the sample. The mean cell size values for the 5 and 10 wt% CNF (Fig. 2) samples were identical within error. The increase in the cell size of the 15 wt% CNF-Clariant system could be due to the markedly higher melt strength [35] and the associated network formation, at this high filler concentration which may hinder the growth of the cells; it is worth noting that samples of this 15 wt% blend were previously found to be brittle when injection moulded [36] and to be unsuitable for fibre-spinning [18], unlike the lower loading fractions. Close inspection of the samples shows that the CNFs were fully incorporated into the cell membranes and struts (Fig. 3) and are mainly aligned in the direction of the elongational flow.

The density of the compact composite blend increases with CNF content (Fig. 4), as expected, since the graphitic material is denser than the matrix polymer. In contrast, the densities of the integral nanocomposite foam samples are up to 20% lower than the pure polymer, despite the higher intrinsic density of the CNFs. Three of the 5 wt% CNF-Clariant samples had the same density as the solid reference, suggesting that no foaming had occurred; these samples were removed from the study. This problem was

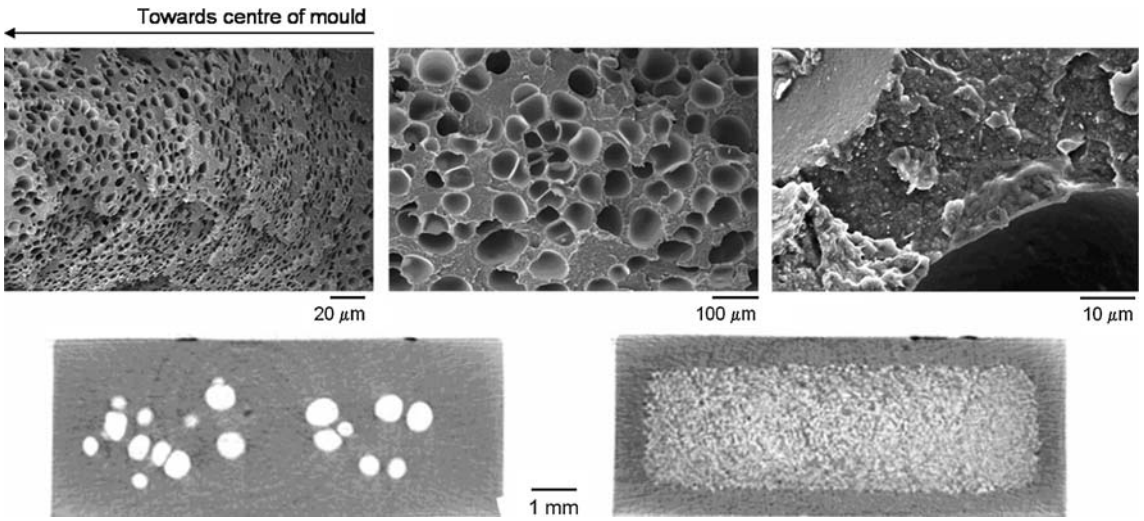

Fig. 3 *Top*: Representative SEM images of the 10 wt% CNF-Clariant foams. *Bottom*: X-ray tomography cross-sections comparing Clariant foam without (*left*) and with 10 wt% (*right*) CNF

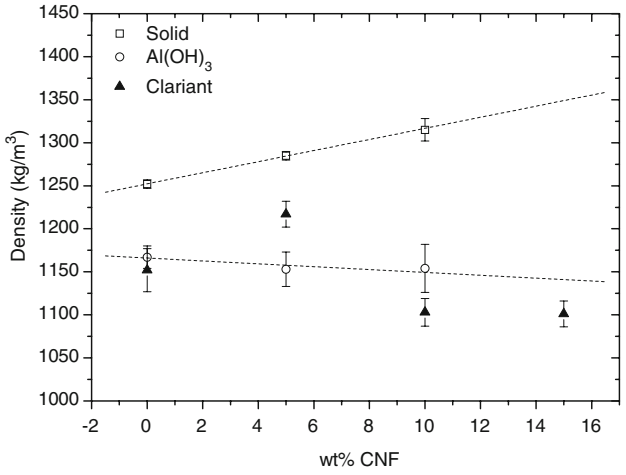

Fig. 4 Average density and standard error as a function of CNF content and blowing agent in the integral PEEK-CNF foams, with linear fits to the solid and $Al(OH)_3$ data

not observed for either the 10 wt% or 15 wt% CNF-Clariant samples, and may be attributed to difficulties feeding the extruder with the small quantities made necessary by the limited availability of CNFs. The $Al(OH)_3$ samples also have a reduced density, despite the increasing CNF content and the decreasing cell size, presumably as bubbles are progressively stabilised (although less effectively than for the Clariant system). The high-quality CNF-Clariant foams show the most pronounced density reduction for the 10 wt% CNF sample; since the cell size is similar to the 5 wt% sample, there must be an increase in volume porosity for 10 wt% CNFs which appears to be the optimally stabilised system.

Figure 5 summarises the average mechanical properties in bending, as a function of the blowing agent type and nanofibre loading. The standard deviation of the elastic modulus and yield strength was less than 1% in both cases, confirming excellent reproducibility. The properties in bending are dominated by the solid skins on the outer surfaces of the samples, with the foamed cores providing a convenient route to density reductions whilst supporting a stable, high bending moment structure. The presence of CNFs increases both the stiffness and the yield strength of all the test bars (foamed and unfoamed) with a slight (10–15%) decrease in the yield strain for the higher loading fraction CNF-Clariant samples; the reduced yield strain correlated with the onset of brittle fracture, perhaps due to a loss of ductility in the filled and drawn struts (see below for a discussion of matrix morphology). Regardless of blowing agent type, the absolute flexural stiffness increases linearly with CNF loading fraction (see Fig. 5), as observed previously in tensile tests of solid samples [36], with a 40% increase at 15wt% CNFs. Here, the similarity of the curves highlights the dominance of the solid skins; however, the

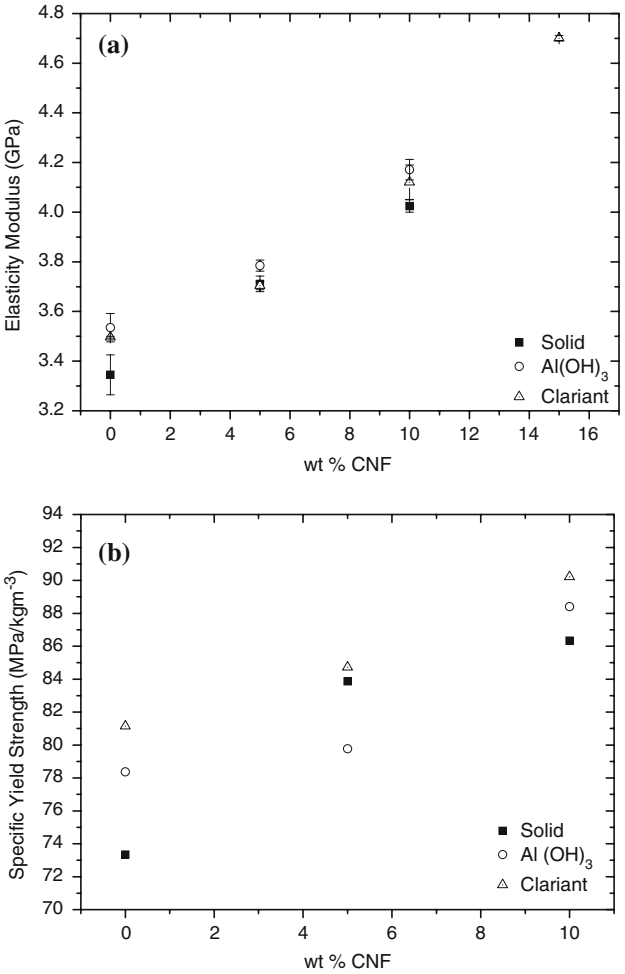

Fig. 5 Mechanical properties in bending as a function of CNF content and blowing agent. **a** Absolute elasticity modulus and **b** Specific yield strength

increase in specific modulus (of up to 59%) is even larger for the foamed samples, due to the associated density reduction. The absolute flexural strengths (defined as the stress where the stress–strain curve deviates from the linear region, not shown) increase on adding CNFs, but are adversely affected by the foamed core; consequently, the largest increases are seen for the solid samples. However, once normalised, the specific flexural strength (Fig. 5b) of the foams shows an increase of 5–10% with respect to the solid bars. The foam structure, with the smallest cells, generated by the Clariant blowing agent, provides the best specific stress performance, at every loading fraction. In short, the addition of CNFs allows the production of foamed PEEK components with greater flexural strength and modulus than pure, solid PEEK, combined with a 20% density reduction.

The compressive behaviour of the foams is shown in Fig. 6 for both the $Al(OH)_3$ and Clariant systems; the foam behaviour was isolated by cutting off the outer skins of the

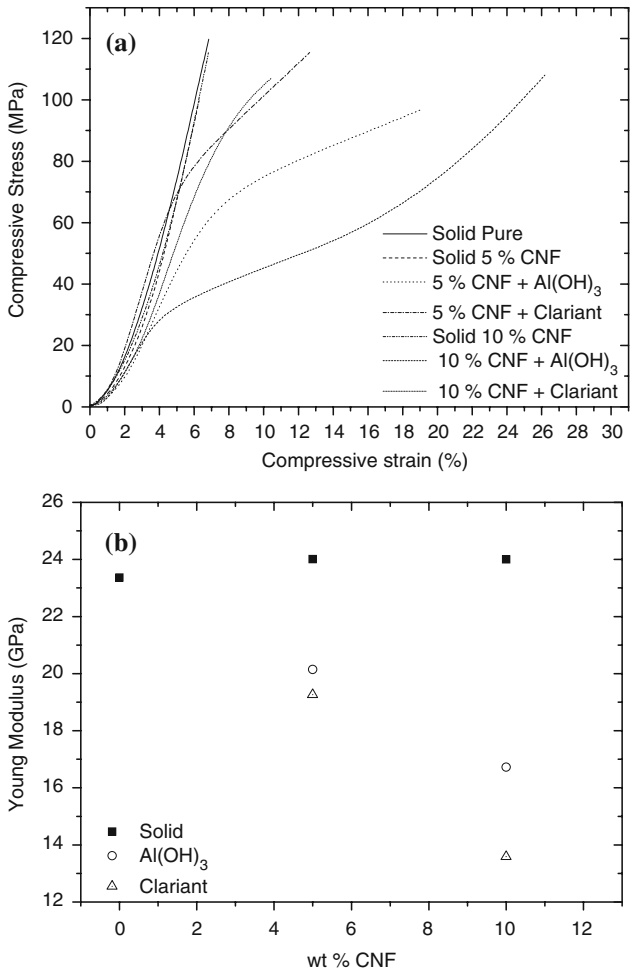

Fig. 6 Compressive stress–strain behaviour for solid and foamed samples and absolute Young's modulus, as a function of CNF content and blowing agent

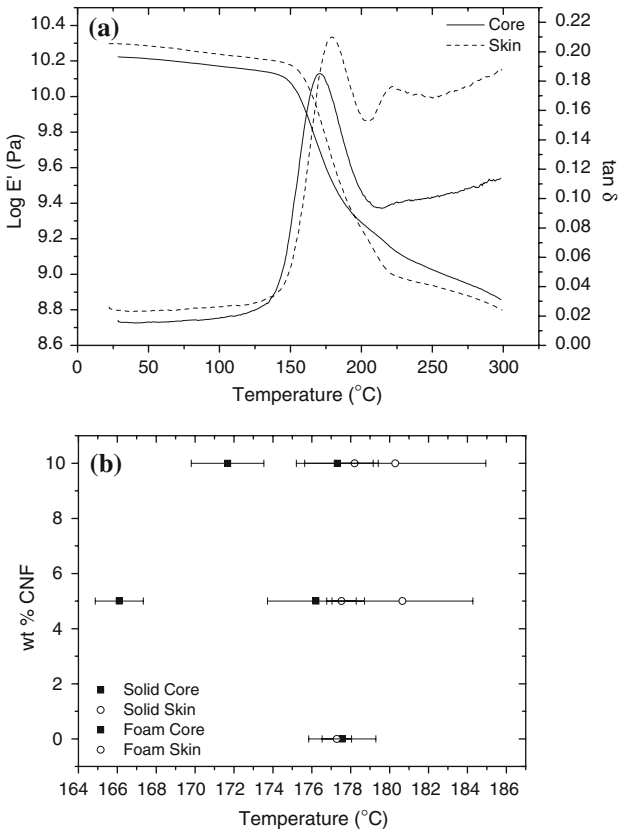

Fig. 7 **a** Representative log storage modulus and tan δ of foam core and skin samples for 10 wt% CNF-Clariant. **b** Glass transition temperature taken from tan δ peak values

samples. As can be seen, the only sample which clearly exhibits the typical compressive behaviour of foams is the 10 wt% CNF-Clariant sample. As noted above, this system was the most successful, showing the highest porosity and smallest average cell size. The other foam samples, containing larger and less uniform cells, only exceeded the yield point and entered the plateau region just before the loading head reached its limit. As expected, the absolute moduli (Fig. 6) of the foams are lower than those of their solid counterparts. It is interesting to note that the presence of the CNFs does not raise the compression modulus, in contrast to the tension and bending results, possibly due to nanofibre buckling.

The bending and damping properties of the more uniform, Clariant foams were assessed using DMTA, by cutting 1-mm thick samples from both the skin and the mould core and removing 0.5 mm from the upper and lower solid layer. The results (Fig. 7) show a decrease in the stiffness of the core and a shift of the glass transition temperature (T_g) towards lower temperatures, as compared to the solid skin. The shift in T_g is greater for the 5 wt% CNF ($\Delta T_g = 11$ °C) than for 10 wt% CNF ($\Delta T_g = 6$ °C) sample (see Fig. 7). The solid and foamed skin samples have transition temperatures that agree within error. That the foamed regions have a lower T_g may be explained by the fact that they experience a high extensional flow whilst cooling rapidly. These conditions generate a high concentration of small crystal nuclei that limit further crystallisation during annealing, leading to a low final degree of crystallinity. Such effects have been observed to reduce significantly the T_g of pure PEEK fibres [18]. On the other hand, the addition of CNFs has been shown to mitigate the effect, increasing the degree of crystallinity and the T_g. The smaller ΔT_g for the higher CNF concentration is consistent with this explanation. The magnitudes of the shifts in the foamed samples are smaller than those reported previously for PEEK fibres, but the cooling rate is slower and the change in crystallinity more modest (as discussed below).

Differential scanning calorimetry analysis was performed on similar samples from the skin and core of the compounds, in order to assess possible differences on their

Table 1 Characteristic parameters of both skin and core samples, established by DSC

Sample	T_m (°C)		T_c (°C)		X_m^c (%)		X_c^c (%)	
	Skin	Core	Skin	Core	Skin	Core	Skin	Core
0% CNF	340	338	299	298	31	29	32	32
5% CNF	338	338	301	301	29	27	35	36
10% CNF	339	339	301	302	30	27	35	36
0% CNF + $Al(OH)_3$	340	338	300	300	29	26	34	34
5% CNF + $Al(OH)_3$	339	340	301	302	29	26	35	34
10% CNF + $Al(OH)_3$	338	339	302	302	29	28	37	36
0% CNF + Clariant	339	338	298	298	29	28	33	34
5% CNF + Clariant	338	338	299	299	29	26	33	32
10% CNF + Clariant	339	338	301	301	28	24	36	36
15% CNF + Clariant	339	338	301	301	30	28	36	36

degree of crystallinity. The melting (T_m) and crystallisation (T_c) temperatures were taken from the peak values of the respective transitions. A small feature around 230 °C can be observed for all the samples due to the annealing treatment but its enthalpy is negligible. The degree of crystallinity was calculated from the main melting and crystallisation enthalpies normalised to the weight fraction of polymer. The results are shown in Table 1. In all cases, both T_c and T_m have identical values for the skin and core samples, within experimental error. Additionally, all the samples from the skin had a degree of crystallinity on melting of 29 ± 1%. However, the degree of crystallinity on melting of the foamed cores varied from 24 to 29%. The finest-celled Clariant cores (10wt% CNF) had the smallest crystallinity, consistent with the discussion of T_g above. The degree of crystallinity on cooling was several degrees higher than that determined from the original melting, due to a more generous cooling rate in the DSC; notably, the suppression of the resulting crystallinity in the foamed region disappears, as expected once the polymer is relaxed. The slight increase in total crystallinity in the presence of CNFs is in agreement with previous results [36] which identified a small broadening of the crystallisation peak in CNF-loaded PEEK nanocomposites; the effect was attributed to an interaction between the nanofibres and the matrix occurring during slow crystallisation.

Conclusions

The addition of CNFs allows straightforward production of uniform, high-quality, PEEK integral foams, using a simple chemical foam injection-moulding technique. The vapour-grown CNFs were homogeneously dispersed and partially aligned in the thermoplastic matrix, following initial extrusion compounding and subsequent moulding. The optimal nanofibre content for foaming of the semicrystalline PEEK was found to be 10 wt%; at this concentration the nanofibres provide an optimum balance between the enhancement of the polymer rheology without excessively limiting the polymer chain mobility. Mechanical testing of the resulting integral foams showed an increase in the flexural elastic modulus and yield strength of the reinforced samples; the specific yield strength of the foams out-performed even the reinforced compact reference samples. These materials are, therefore, very promising for applications that require lightweight but stiff PEEK panels, as the bending stiffness can be maintained with a 20% weight reduction. The study confirms that the improved intrinsic properties of the cellular PEEK are due to the CNFs; some changes in the degree of matrix crystallinity due to the nucleating properties of the nanoscale filler were revealed by DSC but are modest. Indeed, the mechanical performance increased despite a slight reduction in matrix crystallinity of the foam core. This study has, therefore, demonstrated the processability and enhanced properties of a thermoplastic matrix that cannot readily be foamed, and suggests an approach that could be applied to other types of system.

Acknowledgement Raquel Verdejo would like to acknowledge the financial support from the EPSRC.

References

1. Harris PJF (2004) Int Mater Rev 49(1):31
2. Shaffer M, Sandler J (2007) In: Advani S (ed) Processing and properties of nanocomposites. World Scientific, Singapore, Chapter 1, pp 1–59. http://www.worldscibooks.com/nanosci/6317.html
3. Shaffer MSP, Windle AH (1999) Adv Mater 11(11):937
4. Safadi B, Andrews R, Grulke EA (2002) J Appl Polym Sci 84(14):2660
5. Valentini L, Biagiotti J, López-Manchado MA, Santucci S, Kenny JM (2004) Polym Eng Sci 44(2):303

6. Coleman JN, Cadek M, Blake R, Nicolosi V, Ryan KP, Belton C, Fonseca A, Nagy JB, Gun'ko YK, Blau WJ (2004) Adv Funct Mater 14(8):791
7. Raravikar NK (2005) Chem Mater 17(5):974
8. Cadek M, Coleman JN, Ryan KP, Nicolosi V, Bister G, Fonseca A, Nagy JB, Szostak K, Beguin F, Blau WJ (2004) Nano Lett 4(2):353
9. Coleman JN, Blau WJ, Dalton AB, Munoz E, Collins S, Kim BG, Razal J, Selvidge M, Vieiro G, Baughman RH (2003) Appl Phys Lett 82(11):1682
10. Lahiff E, Ryu CY, Curran S, Minett AI, Blau WJ, Ajayan PM (2003) Nano Lett 3(10):1333
11. Olek M, Ostrander J, Jurga S, Mohwald H, Kotov N, Kempa K, Giersig M (2004) Nano Lett 4(10):1889
12. Wang Z, Liang Z, Wang B, Zhang C, Kramer L (2004) Compos Part A: Appl Sci Manuf 35(10):1225
13. Zhang X, Liu T, Sreekumar TV, Kumar S, Moore VC, Hauge RH, Smalley RE (2003) Nano Lett 3(9):1285
14. Liu T, Kumar S (2003) Nano Lett 3(5):647
15. Finegan IIC (2003) J Mater Sci 38(16):3485. doi:10.1023/A:1025109103511
16. Gao J, Itkis ME, Yu A, Bekyarova E, Zhao B, Haddon RC (2005) J Am Chem Soc 127(11):3847
17. Ma H, Zeng J, Realff ML, Kumar S, Schiraldi DA (2003) Compos Sci Technol 63(11):1617
18. Sandler J, Windle AH, Werner P, Altstadt V, Es MV, Shaffer MSP (2003) J Mater Sci 38(10):2135. doi:10.1023/A:1023715811817
19. Sandler JKW, Pegel S, Cadek M, Gojny F, van Es M, Lohmar J, Blau WJ, Schulte K, Windle AH, Shaffer MSP (2004) Polymer 45(6):2001
20. Klempner D, Frisch KC (1991) Handbook of polymeric foams and foam technology. Hanser Publishers, New York
21. Yuan MJ, Turng LS, Gong SQ, Caulfield D, Hunt C, Spindler R (2004) Polym Eng Sci 44(4):673
22. Kharbas H, Nelson P, Yuan MJ, Gong SQ, Turng LS, Spindler R (2003) Polym Compos 24(6):655
23. Mahfuz H, Rangari VK, Islam MS, Jeelani S (2004) Compos Part A: Appl Sci Manuf 35(4):453
24. Han XM, Zeng CC, Lee LJ, Koelling KW, Tomasko DL (2003) Polym Eng Sci 43(6):1261
25. Nam PH, Maiti P, Okamoto M, Kotaka T, Nakayama T, Takada M, Ohshima M, Usuki A, Hasegawa N, Okamoto H (2002) Polym Eng Sci 42(9):1907
26. Tomasko DL, Han XM, Liu DH, Gao WH (2003) Curr Opinion Solid State Mater Sci 7(4–5):407
27. Zeng CC, Han XM, Lee LJ, Koelling KW, Tomasko DL (2003) Adv Mater 15(20):1743
28. Ema Y, Ikeya M, Okamoto M (2006) Polymer 47(15):5350
29. Fujimoto Y, Ray SS, Okamoto M, Ogami A, Yamada K, Ueda K (2003) Macromol Rapid Commun 24(7):457
30. Shen J, Zeng C, Lee LJ (2005) Polymer 46(14):5218
31. Yang Y, Gupta MC, Dudley KL, Lawrence RW (2005) Adv Mater 17(16):1999
32. Yang Y, Gupta MC, Dudley KL, Lawrence RW (2005) Nano Lett 5(11):2131
33. Yang Y, Gupta MC, Dudley KL, Lawrence RW (2004) Nanotechnology 15(11):1545
34. Lee LJ, Zeng C, Cao X, Han X, Shen J, Xu G (2005) Compos Sci Technol 65(15–16):2344
35. Werner P, Verdejo R, Wöllecke F, Altstädt V, Sandler JKW, Shaffer MSP (2005) Adv Mater 17(23):2864
36. Sandler J, Werner P, Shaffer MSP, Demchuk V, Altstadt V, Windle AH (2002) Compos Part A: Appl Sci Manuf 33(8):1033
37. Werner P, Altstadt V, Jaskulka R, Jacobs O, Sandler JKW, Shaffer MSP, Windle AH (2004) Wear 257(9–10):1006
38. McGrum NG, Buckley CP, Bucknall CB (1988) Principles of polymer engineering. Oxford University Press, UK